Neuron, Vol. 28, 287–298, October, 2000, Copyright ©2000 by Cell Press

Adaptation-Induced Plasticity of Orientation Tuning in Adult Visual Cortex

Valentin Dragoi,* Jitendra Sharma, and Mriganka Sur
Department of Brain and Cognitive Sciences
Massachusetts Institute of Technology
Cambridge, Massachusetts 02139

Summary

A key emergent property of the primary visual cortex (V1) is the orientation selectivity of its neurons. The extent to which adult visual cortical neurons can exhibit changes in orientation selectivity is unknown. Here we use single-unit recording and intrinsic signal imaging in V1 of adult cats to demonstrate systematic repulsive shifts in orientation preference following short-term exposure (adaptation) to one stimulus orientation. In contrast to the common view of adaptation as a passive process by which responses around the adapting orientation are reduced, we show that changes in orientation tuning also occur due to response increases at orientations away from the adapting stimulus. Adaptation-induced orientation plasticity is thus an active time-dependent process that involves network interactions and includes both response depression and enhancement.

Introduction

V1 neurons are selective for the orientation of lines that are presented in their receptive field center (Hubel and Wiesel, 1962). The development of orientation tuning does not require visual experience (Hubel and Wiesel, 1963; Fregnac and Imbert, 1978; Godecke et al., 1997; Crair et al., 1998), although selective experience in early life can modify the orientation preference of neurons (Blakemore and Cooper, 1970; Hirsch and Spinelli, 1970; Blakemore, 1977; Stryker et al., 1978; Sengpiel et al., 1999). Orientation selectivity arises within V1 due to influence from thalamic afferents (Ferster, 1986; Chapman et al., 1991; Reid and Alonso, 1995; Ferster et al., 1996), with a postulated role for intracortical circuitry in enhancing the bias provided by thalamic inputs (Benevento et al., 1972; Sillito et al., 1980; Worgotter and Koch, 1991; Ben-Yishai et al., 1995; Douglas et al., 1995; Somers et al., 1995). Consistent with the latter view, orientation tuning of adult V1 neurons evolves dynamically after a latency of about 40 ms (Celebrini et al., 1993; Shevelev et al., 1993; Ringach et al., 1997). However, the steady-state orientation preference of adult neurons is considered to be a stable property that remains fundamentally unchanged after early life. In counterpoint to this belief are well-known psychophysical phenomena reporting temporal contextual effects on the perception of orientation (Gibson, 1933; Gibson and Radner, 1937; Magnussen and Kurtenbach, 1980; Wolfe, 1984; Greenlee and Magnussen, 1987). These phenomena raise the question of whether orientation selectivity in adult V1 can undergo changes induced by temporal context. Therefore, we examined here the plasticity of orientation tuning, using pattern adaptation (Movshon and Lennie, 1979; Saul and Cynader, 1989; Carandini et al., 1998) as the induction procedure, by analyzing how the entire profile of the orientation tuning curve changes after short- and long-term adaptation to a particular stimulus orientation.

*To whom correspondence and requests for materials should be addressed (e-mail: vdragoi@ai.mit.edu).

Results

We measured the orientation tuning curve of neurons before and after adaptation to an oriented grating stimulus and after recovery from adaptation (Figure 1A). Figure 1B demonstrates the stimulus dependence of adaptation by showing how the preferred orientation of a representative cell changes after 2 min of exposure to one orientation located on one flank of the cell's tuning curve, followed by a period of recovery, subsequent adaptation to a different orientation located on the opposite flank with respect to the preferred orientation, and a final period of recovery. When the difference between the cell's preferred orientation and that of the adapting stimulus ($\Delta\theta$) is $-22.5°$, there is a shift in preferred orientation to the right, away from the adapting stimulus. In contrast, when the adapting stimulus is presented on the right flank of the tuning curve ($\Delta\theta = 45°$), the preferred orientation shifts to the left and then returns to the original value after 10 min of recovery. In both postadaptation conditions, there is a decrease in response at the preadaptation-preferred orientation and a broadening of tuning.

The interesting effect in Figure 1B is that exposure to particular orientations reveals an active process of plasticity by which responses on the flank of the tuning curve near the adapting orientation are depressed, whereas responses on the opposite flank are enhanced. However, adaptation to stimuli orthogonal to the cell's preferred orientation ($\Delta\theta$ between 60° and 90°) induces little change in preferred orientation. Figure 1C illustrates the behavior of one representative cell that exhibits a stimulus-dependent shift after 2 min of adaptation to a 22.5° stimulus, but the orientation preference remains unchanged when $\Delta\theta$ is 90°.

To characterize the plasticity of orientation tuning, we determined quantitatively the relationship between $\Delta\theta$ and changes in preferred orientation for the population of cells ($n = 130$). Figure 1D shows the relation between the magnitude of the shift in optimal orientation and $\Delta\theta$ (positive shifts are shown as repulsive with respect to the adapting orientation). For each cell, we evaluated whether a shift in preferred orientation was significant ($p < 0.05$, Student's t test) based on a trial-by-trial comparison between control and adaptation conditions. Thus, when $\Delta\theta$ is in the range 0°–30°, 79% of cells (30 of 38) show significant repulsive shifts in orientation,

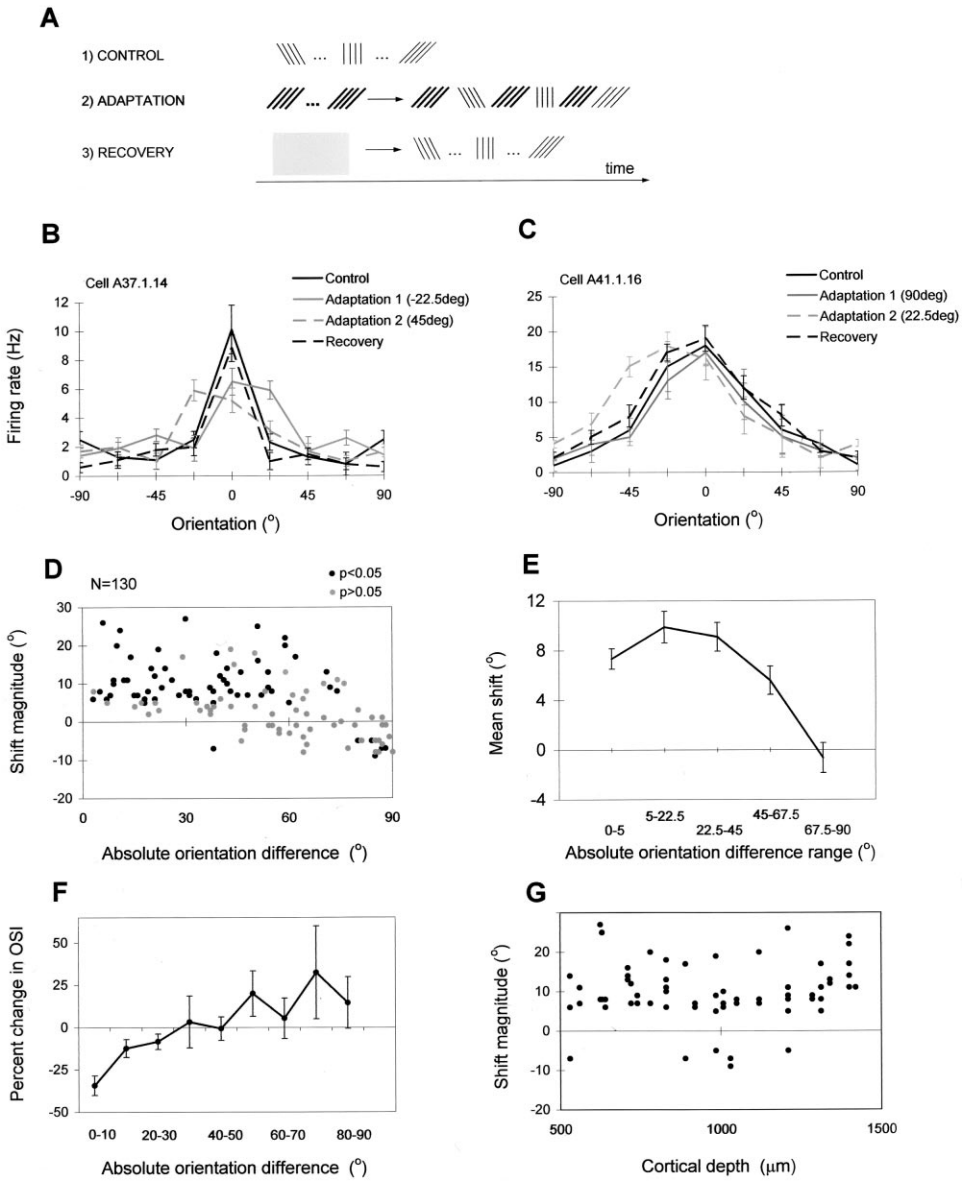

Figure 1. Adaptation-Induced Plasticity of Orientation Tuning in V1 Cells

(A) The control, adaptation, and recovery protocols. Drifting gratings of random orientations between 0° and 180° (resolution 22.5°) and two directions of movement were presented binocularly during the following conditions (see Experimental Procedures): (1) control, each grating was presented for 2.5 s and data collected for the "control" tuning curve; (2) adaptation, an initial block of continuous adaptation to one grating of fixed orientation was followed by random presentations of the 16 gratings (2.5 s each presentation) and data collected for the "adaptation" tuning curve—during data collection, each grating was preceded by a 5 s "topping-up" presentation of the adapting orientation (bold lines); (3) recovery, a 10 min period of recovery with a full-field uniform stimulus (gray rectangle) was followed by random presentations of the 16 gratings (in conditions identical to the control) and data collected for the "recovery" tuning curve.

(B and C) Orientation tuning curves of two representative cells that were successively adapted to two different orientations. Each graph represents orientation tuning during four conditions: control (black), adaptation to the first orientation (solid gray), adaptation to the second orientation (dashed gray), and recovery (black, dashed line). In our tuning curve display convention, the control optimal orientation is represented as 0°, and all subsequent tuning curves (during adaptation and recovery) are represented relative to the control condition.

(D) Scatter plot ($n = 130$ cells) showing the magnitude of the postadaptation shift in preferred orientation (positive numbers indicate repulsive shifts, whereas negative numbers indicate attractive shifts) as a function of the absolute difference between the adapting orientation and the control-preferred orientation ($\Delta\theta$). Cells that show significant shifts in preferred orientation based on a trial-by-trial comparison during adaptation and control conditions are shown in black ($p < 0.05$); those that do not show significant shifts are shown in gray ($p > 0.05$).

(E) Mean shift magnitude as a function of $\Delta\theta$ ($n = 130$ cells). Cells with both significant and nonsignificant shifts in orientation are included.

(F) Postadaptation changes in orientation selectivity index (OSI). For $\Delta\theta$ in the range 0°–30°, 26 of 38 cells show a decrease in their orientation selectivity index, whereas only 5 cells show an increase. When $\Delta\theta$ is in the range 30°–60°, 16 of 49 cells show a decrease in orientation selectivity index, whereas 14 cells show an increase. When $\Delta\theta$ is in the range 60–90°, 17 of 43 cells show an increase in orientation selectivity, whereas 10 show a decrease. The graphs in (B), (C), (E), and (F) represent mean values ± SEM.

(G) Relationship between the shift magnitude and cortical depth for all the neurons exhibiting significant shifts in orientation magnitude.

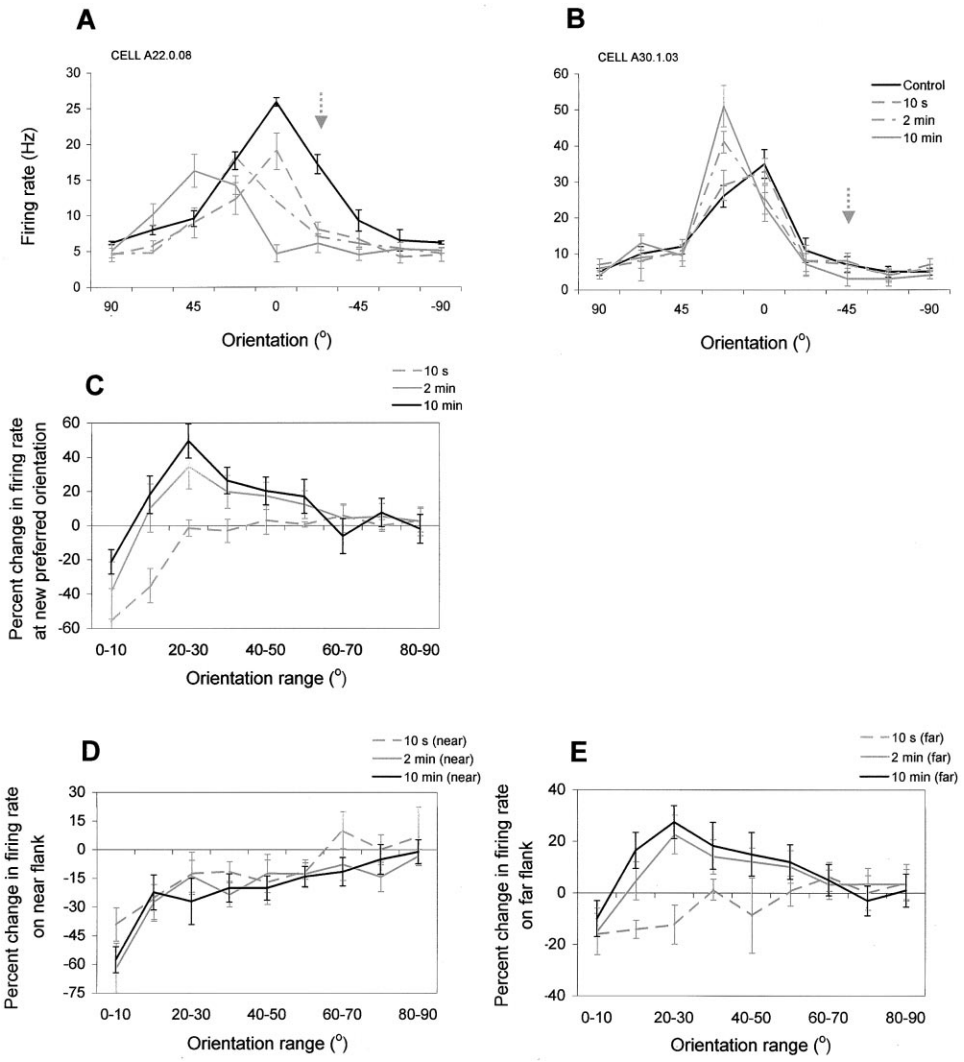

Figure 2. Adaptation-Induced Response Suppression and Facilitation

(A and B) Tuning curves of cells that show adaptation-induced response suppression on the near flank and response facilitation on the far flank. Each cell was successively exposed to different adaptation periods: 10 s, 2 min, and 10 min. Tuning curves were calculated in each of the four conditions: control (black), 10 s adaptation (gray, dashed line), 2 min adaptation (gray, dotted line), and 10 min adaptation (gray, solid line). The adapting orientation is marked by the gray arrow.

(C) Percent change in firing rate of the response at the new preferred orientation. Cells were divided into nine subpopulations depending on the difference between each cell's preferred orientation (before adaptation) and that of the adapting stimulus.

(D) Percent change in firing rate of responses on the near flank of the tuning curve relative to the adapting orientation.

(E) Percent change in firing rate of responses on the far flank of the tuning curve relative to the adapting orientation. Each graph represents mean values ± SEM.

whereas no cell shows an attractive shift; when $\Delta\theta$ is in the range 30°–60°, 53% of cells (26 of 49) show significant repulsive shifts in orientation, and only one cell shows an attractive shift; when $\Delta\theta > 60°$, 11% of cells (5 of 43) show a repulsive shift, and 14% of cells (6 of 43) show an attractive shift in orientation preference. The fraction of cells showing significant repulsive shifts in preferred orientation decreases as $\Delta\theta$ increases (correlation coefficient $r = -0.99$, $p < 0.00005$, Pearson test).

The mean shift magnitude histogram (Figure 1E) was obtained by pooling cells into four bins (the first bin was divided into two $\Delta\theta$ ranges: 0°–5° and 5°–22.5°). This figure shows that the magnitude of the repulsive shift tends to increase as $\Delta\theta$ increases from 0° to 22.5°, followed by a decay to 0° as $\Delta\theta$ approaches 90°. For the entire population of cells ($\Delta\theta$ range 0°–90°), there is a significant inverse relationship between the shift magnitude and $\Delta\theta$ (correlation coefficient $r = -0.52$, $p < 0.0005$, Pearson test).

In addition to the shift in orientation, adaptation reduces the response magnitude of V1 neurons measured at the control optimal orientation. The reduction in firing rate, measured at the control-optimal orientation, is >40% for orientation differences <10° ($p < 0.05$, t test). As $\Delta\theta$ increases, the depression in firing rate becomes smaller until it reaches 0 when $\Delta\theta$ approaches 50°. There

Table 1. Cells Showing Adaptation-Induced Suppression and Facilitation at the New Preferred Orientation

Adaptation Time	Δθ: 0°–22.5°		Δθ: 22.5°–45°		Δθ: 45°–67.5°		Δθ: 67.5°–90°	
	Suppression	Facilitation	Suppression	Facilitation	Suppression	Facilitation	Suppression	Facilitation
10 s	12/15	1/15	11/21	2/21	3/17	4/17	0/14	0/14
2 min	12/26	7/26	4/29	19/29	2/23	15/23	2/14	2/14
10 min	7/18	3/18	2/19	13/19	1/18	12/18	1/12	1/12

Adaptation-induced suppression and facilitation at the new preferred orientation. Δθ is the absolute difference between each cell's preferred orientation and that of the adapting stimulus. The numbers in each box represent the ratio between the number of cells showing a statistically significant suppressive or facilitatory effect versus the total number of cells for each condition. For instance, 12 out of 15 cells showed statistically significant response suppression at the new preferred orientation after 10 s of adaptation for a Δθ range between 0° and 22.5°. This analysis was performed on a population of 92 neurons that were serially exposed to different adaptation periods (10s, 2 min, and 10 min) at a broad range of Δθs.

is a significant inverse relationship between the decrease in firing rate and Δθ (correlation coefficient $r = -0.39$, $p < 0.0005$, Pearson test).

The plasticity of orientation tuning also includes changes in the tuning strength (width), calculated here as the orientation selectivity index (OSI). At the orientation differences at which we found large shifts in preferred orientation ($\Delta\theta < 60°$), cells broaden their orientation selectivity (Figure 1F), i.e., their (OSI) decreases. However, for $\Delta\theta > 60°$ there is a tendency for the (OSI) to increase, although this sharpening of tuning is not statistically significant ($p > 0.1$, Student's t test). For the full range of Δθ, there is a significant relationship between orientation tuning strength and Δθ (correlation coefficient $r = 0.294$, $p < 0.0005$, Pearson test). Together with the enhancement of responses on the far flank of the tuning curve (see below), the sharpening of tuning at large Δθ is consistent with a process by which responses at a broad range of orientations reorganize after adaptation.

Given the vastly different inputs and outputs of neurons in different cortical layers that can impose restrictions on the orientation specificity of adaptation, it is possible that the magnitude of the shift in orientation tuning is related in some way to the recording depth. While we did not assign cells to individual layers, there was no tendency for adaptation effects to differ as a systematic function of cortical depth. Thus, Figure 1G represents the magnitude of the significant shifts in preferred orientation ($p < 0.05$) as a function of cortical depth for the whole population of neurons. The scatter plot shows that there is no relationship between the orientation shift and cortical depth (correlation coefficient $r = 0.088$, $p > 0.1$, Pearson test), suggesting that the observed changes in orientation selectivity constitute a property of cortical neurons and their local connections rather than the extent of receptive field integration.

To investigate the emergence of the adaptation-induced response suppression on the near flank (defined by responses on the half of the tuning curve toward the adapting orientation, including the control preferred orientation) and response facilitation on the far flank (defined by the rest of responses on the other half of the tuning curve, excluding the control preferred orientation), we successively exposed V1 neurons to different adaptation periods: 10 s, 2 min, and 10 min. Figures 2A and 2B shows two cells that exhibit significant shifts in orientation following adaptation to stimuli oriented 22.5° (Figure 2A) and 45° (Figure 2B) away from the cell's peak orientation. Both the response reduction on the near flank and facilitation on the far flank build up gradually in time: increasing the adaptation time from 10 s to 10 min shows a progressive depression of responses on the near flank and a progressive facilitation of responses on the far flank. For the largest adaptation period (10 min), we found that many cells increase their response at the new preferred orientation by a factor of 2 or more (e.g., Figure 2B). Importantly, the orientation at which the adapting stimulus is presented elicits weak or no responses under the various time periods from the two cells shown in Figures 2A and 2B (except for the control condition tuning curve shown in Figure 2A). Yet, adaptation induces a significant shift in optimal orientation, along with the reorganization of responses around the new preferred orientation.

Figure 2C shows that the increase in response at the new preferred orientation builds in time with continuous adaptation and is also a function of Δθ. After 10 s of adaptation, the response at the new preferred orientation is suppressed relative to the control response at small Δθ, with little effect at larger Δθ (>30°). However, as adaptation time increases, tuning curves are remodeled: there is less suppression at small Δθ (0°–20°), marked facilitation at intermediate Δθ (20°–60°; $p < 0.05$, Student's t test, comparing responses in each bin at 2 and 10 min with those in the control condition), and no effect at high Δθ (60°–90°; $p > 0.05$)—the population data are summarized in Table 1. Although suppression dominates after 10 s of adaptation, after 10 min the resultant facilitation becomes stronger than the suppression observed at small Δθ s. Importantly, the supraoptimal facilitatory effects are highly reliable for a large range of Δθs (between 20° and 60°) after both 2 and 10 min of adaptation. Thus, orientation plasticity involves an active process of network synaptic changes that lead to a new preferred orientation rather than simply a passive reduction of orientation selective responses around the adapting orientation.

To quantify the adaptation-induced changes in responses at all orientations, we calculated, for the entire population of cells, the mean change in firing rate on the near and far flanks as a function of Δθ (Figures 2D and 2E). Confirming previous adaptation studies (e.g., Blakemore and Campbell, 1969; Saul and Cynader, 1989; Nelson, 1991; Carandini et al., 1998), we found that

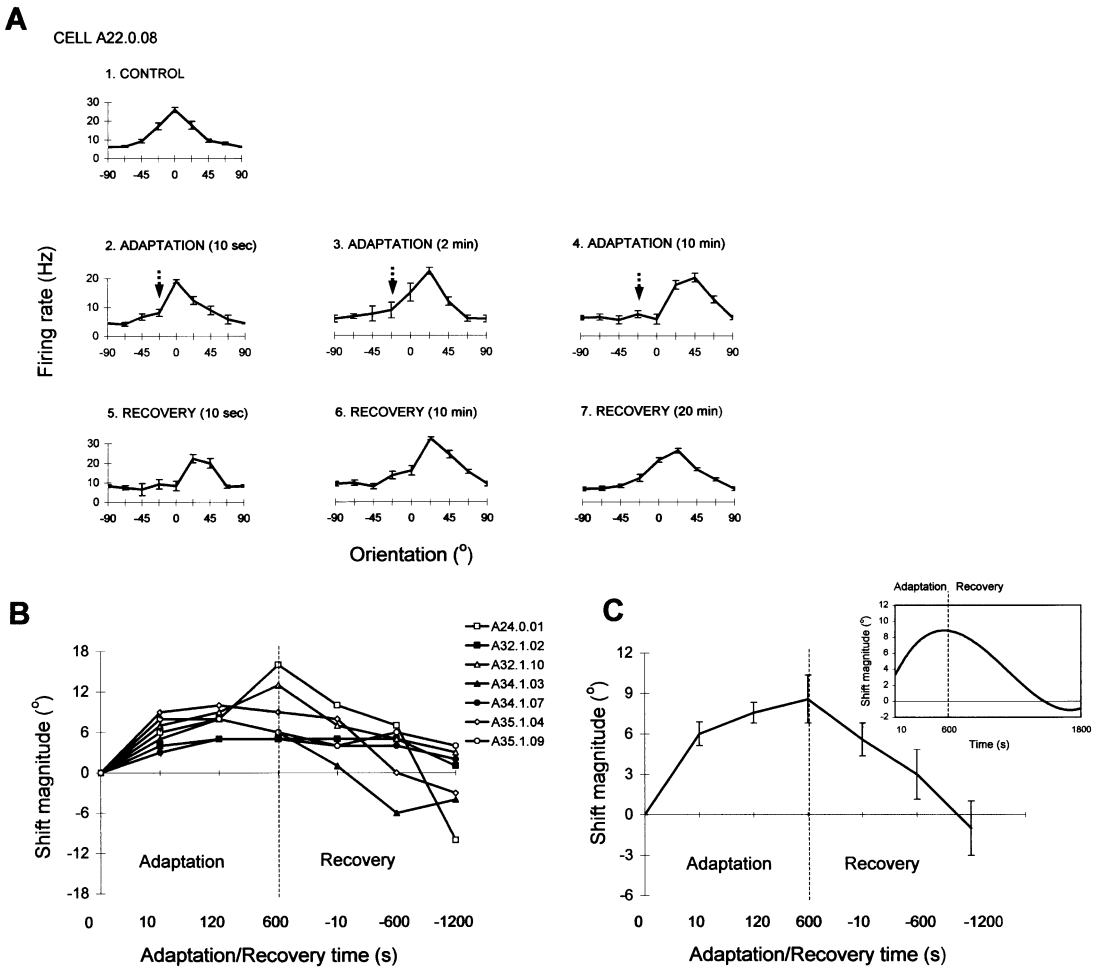

Figure 3. Time Course of Orientation Adaptation and Recovery

(A) One cell that shows large changes in preferred orientation during adaptation and recovery. Each graph represents the orientation tuning curve at the following stages: (1) control condition; (2) adaptation to -22.5° for 10 s; (3) adaptation to -22.5° for 2 min; (4) adaptation to -22.5° for 10 min; (5) recovery for 10 s; (6) recovery for 10 min; (7) recovery for 20 min. During adaptation, the orientation tuning was evaluated based on random presentations of the 16 gratings for 5–7 trials each, preceded by the presentation of the 5 s topping-up adapting stimulus. During control and recovery, the 16 gratings were presented randomly for 7–10 trials each. The adapting orientation is marked by the arrow.

(B) Time course profile of the shift in preferred orientation for seven representative cells (that exhibit significant repulsive shifts in their preferred orientation) during the following conditions: (1) control condition ("0" on the x axis); (2) adaptation for 10 s ("10" on the x axis); (3) adaptation for 2 min ("120" on the x axis); (4) adaptation for 10 min ("600" on the x axis); (5) recovery for 10 s ("-10" on the x axis); (6) recovery for 10 min ("-600" on the x axis); (7) recovery for 20 min ("-1200" on the x axis). Absolute differences between the adapting orientation and each cell's preferred orientation are as follows: A24.0.01 (42°), A32.1.02 (17°), A32.1.10 (61°), A34.1.03 (4°), A34.1.07 (18°), A35.1.04 (9°), and A35.1.09 (31°).

(C) Mean shift magnitude $\pm$ SEM as a function of adaptation and recovery time for the seven cells shown at left. Inset, time course profile of adaptation and recovery for the average data shown in (C), plotted on a linear time scale after fitting the data with a third order polynomial function.

the maximum response suppression occurs for small $\Delta\theta$ values, and this effect dissipates at large orientation differences (Figure 2D). This result was consistent for all adaptation periods. In contrast, responses on the flank of the tuning curve away from the adapting orientation are depressed following 10 s of adaptation, while adaptation for 2 min or more facilitates responses (Figure 2E). The maximum response facilitation is obtained for $\Delta\theta$ in the range 20°–60° ($p < 0.05$, comparing responses in each bin at 2 and 10 min with those in the control condition), and the strength of facilitation decreases as $\Delta\theta$ approaches 90° ($p > 0.05$). As an effect of changing the balance between responses on the near versus far flank of the orientation tuning curve, the magnitude of the repulsive shift in optimal orientation increases with adaptation time, returning to the control value after recovery.

We examined the time course of adaptation and recovery by successively exposing the same cell to adaptation and recovery sessions of different durations: 10 s, 2 min, and 10 min of adaptation, and 10 s, 10 min, and 20 min of recovery, respectively (Figure 3). Figure 3A shows a cell that exhibits a significant shift in orientation following adaptation to a stimulus oriented 22.5° away from the cell's peak orientation. The cell recovers after the last recovery stage (20 min) to a value close to the

original preferred orientation. In Figure 3B we plot the time course of adaptation and recovery by examining the magnitude of shift for seven cells that showed significant changes in their optimal orientation. As the averaged data (Figure 3C) indicates, adaptation and recovery develop at two different time scales, with the rate of recovery being at least an order of magnitude slower than the rate of adaptation (Figure 3C, inset). We estimated the time course of the change in preferred orientation during adaptation and recovery in two ways: (1) calculating the slope of the linear regression line through the adaptation and recovery data points shows that the rate of recovery is 11.9 times slower than the rate of adaptation; (2) fitting the adaptation and recovery curves with a single exponential each shows that the time constant of recovery is 45.4 times the time constant of adaptation.

In order to obtain simultaneously information from large populations of neurons, we next investigated plasticity in orientation tuning by carrying out optical imaging of intrinsic signals from an expanse of V1. Figure 4A shows three composite orientation preference maps from one animal, combining response images at eight different stimulus orientations, obtained during control, adaptation, and recovery conditions. The adapting orientation was fixed throughout the experiment at 135° (Figure 4A, dark green bar). We determined the change in cortical responses induced by the adapting stimulus by computing the difference in orientation preference between control, adaptation, and recovery conditions for each pixel. If the adapting orientation shifts the preferred orientation of cells, pixels flanking the adapting orientation would change their vector angle away from the adapting orientation (dark green). For example, most pixels preferring 112.5° (light green) would shift toward 90° (yellow), and the 90° pixels would shift toward 67.5° (orange), etc. At the opposite side of the adapting orientation, most pixels preferring 157.5° (light blue) would shift toward 180° (dark blue), and the 180° (or 0°) pixels would shift toward 22.5° (purple), etc. Pixels whose orientation preference exactly matches that of the adapting stimulus, e.g., 135° (dark green), would show minimal changes in their angle; others with actual preferred orientation close to 135° (135° $\pm$ 11.25°) would also shift repulsively with respect to the adapting orientation. Finally, if the shift is reversible, all pixels should revert to their initial orientation after recovery from adaptation. Figure 4B shows a magnified portion from Figure 4A that captures the repulsive shift in orientation during adaptation and then shows that most pixels recover to their original orientation.

The change in orientation for each pixel during adaptation and recovery was quantified by calculating the difference between the vector angle of each pixel before and after adaptation, and before adaptation and after recovery. Figure 4C demonstrates that a repulsive shift in orientation follows adaptation. There is a positive change in orientation when the difference between each pixel's orientation and the adapting orientation is positive, and a negative change in orientation when the difference between each pixel's orientation and the adapting orientation is negative ($p < 10^{-19}$, Student's t test). Figure 4C shows that as the orientation difference increases from 0° to $\pm$22.5°, the repulsive shift increases, and this effect diminishes as the orientation difference approaches $\pm$90°. During recovery there is a reversal toward original (control) pixel values. Figure 4D shows in greater detail the changes in individual orientation domains within a representative patch in the control map. Each histogram shows the percentage of pixels within a given orientation domain as a function of orientation shift during adaptation and recovery. In agreement with the single-unit data, Figure 4D shows that for both positive and negative differences between each domain's orientation and the adapting orientation, the orientation shift of pixels is maximal for small to intermediate $\Delta\theta$ and then reduces in magnitude as $\Delta\theta$ approaches 90°.

Interestingly, adaptation not only reorganizes the orientation preference of large individual domains, it can also shift the location of pinwheel centers. Figure 4A shows that, after adaptation, most pinwheel centers change their location and then return toward the control spatial coordinates after recovery. This effect is due to the orientation specificity of adaptation that postulates that only pixels with preferred orientations within a certain $\Delta\theta$ range should exhibit large shifts in orientation (Figure 4C). This orientation asymmetry is commensurate with a shift in the location of pinwheel centers. For instance, Figure 4B details how the pinwheel center in the upper left corner of the control composite map (Figure 4A) shifts its location to the right, mainly by expansion of the 90° (yellow), 112° (light green), 157° (light blue), and 0° (dark blue) orientation domains into the 135° (dark green) region.

We used the images in response to single-stimulus orientations to analyze the changes in optical signal strength and pixel orientation tuning curves before and after adaptation. Figure 5A (from a different animal than Figure 4) shows single-condition responses at four orientations obtained during control, adaptation, and recovery. Using the orientation preference map displayed in Figure 5B, we determined orientation tuning curves for both individual pixels and orientation domains by calculating orientation-dependent changes in the optical signal, before and after adaptation to a stimulus oriented at 135°. Figure 5B shows that the orientation preference of pixels exhibits the same type of changes as shown by individual neurons (Figures 1 and 2). Figure 5C shows the change in signal strength for each set of orientation domains from the entire composite map and demonstrates that responses on the flank of the tuning curve near the adapting stimulus are depressed whereas responses on the far flank are facilitated ($p < 10^{-24}$, Student's t test, comparing pooled near and far flank responses with those during the control condition). To directly link imaging and single-cell data, we performed single-cell recordings after 1 hr of continuous adaptation, for a duration identical to the imaging experiments. In these cells ($n = 27$), Figure 5D shows that such long-term adaptation induces similar repulsive shifts in preferred orientation. For cells that show significant shifts in preferred orientation ($p < 0.05$, Student's t test), there is a greater shift at low $\Delta\theta$ that gradually decreases in magnitude as $\Delta\theta$ approaches 90° (correlation coefficient $r = -0.499$, $p < 0.01$, Pearson test). Consistent with the optical imaging results (Figure 5B), long-term adaptation causes the suppression of responses on the near flank

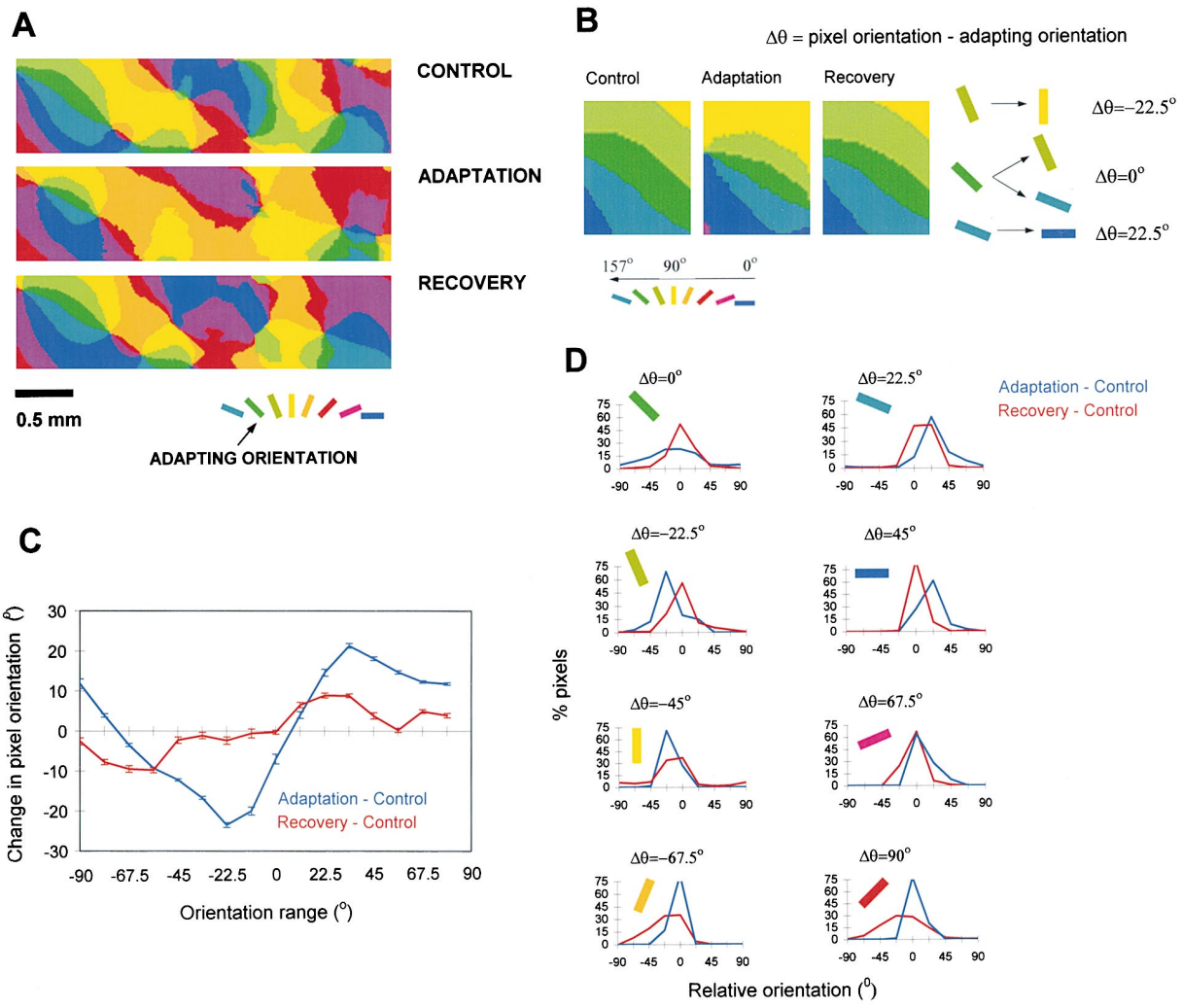

Figure 4. Changes in Orientation Tuning in an Expanse of V1 Demonstrated by Optical Imaging

(A) Composite maps of orientation angle obtained during control, adaptation, and recovery conditions. Data analysis was performed using original, unfiltered, single-orientation maps in all three conditions. To obtain these composite maps we summed vectorially the response at each pixel to the eight single-stimulus orientations (including both directions of motion) and displayed the resultant angle of preferred orientation in pseudocolor according to the key at bottom. Each map was smoothed using a low-pass filter, 5 × 5 kernel size. Adapting orientation is coded dark green.

(B) Magnified portion from (A), showing the postadaptation repulsive shift in orientation and the recovery from adaptation. Depending on the difference between pixel orientation and that of the adapting stimulus ($\Delta\theta$), orientation domains exhibit repulsive shift toward neighboring orientations: for $\Delta\theta = -22.5°$ (light green) most pixels shift toward the "yellow" domain; for $\Delta\theta = 0°$ (dark green) many pixels are unchanged while others shift either toward the "light green" or "light blue" domain; for $\Delta\theta = 22.5°$ (light blue) most pixels shift toward the "dark blue" domain.

(C) Change in pixel orientation during adaptation and recovery. Orientation changes were calculated for all pixels in the entire map of Figure 4A by subtracting the pixel vector angle in the control map from that of the corresponding pixel in the adaptation or the recovery map. We divided all pixels into 16 bins that are represented, relative to the adapting orientation (135°), as the following intervals: [−90°, −78.75°], [−78.75°, −67.5°]…[78.75°, 90°]. Each of these bins is represented on the abscissa (Figure 4C) by the lower bound of each orientation interval. The numbers of the y axis represent the average change in pixel angle.

(D) Histograms of changes in individual orientation domains in the maps of Figure 4A (the analysis was performed on a patch of 66 × 130 pixels starting from the upper left corner of the map). Percentage pixels were calculated by counting the pixels in the control map that shifted to different orientation domains during adaptation and recovery. For display purposes, each orientation domain was centered at 0°, and all changes were calculated relative to the control orientation. We compared adaptation versus control (blue) and recovery versus control (red) conditions. Pixel orientations shift maximally for small $\Delta\theta$, with the shift in general becoming progressively smaller as $\Delta\theta$ approaches 90°. The orientation of each domain is coded as per the key displayed in panels (A) and (B).

and facilitation on the far flank of the tuning curve ($p < 0.05$, Student's t test, comparing postadaptation responses at $\Delta\theta$ in each bin between 0° and 67.5° with those in the control condition; Figure 5E).

Discussion

Our results provide clear evidence that the orientation-selective responses of adult V1 cells are reorganized

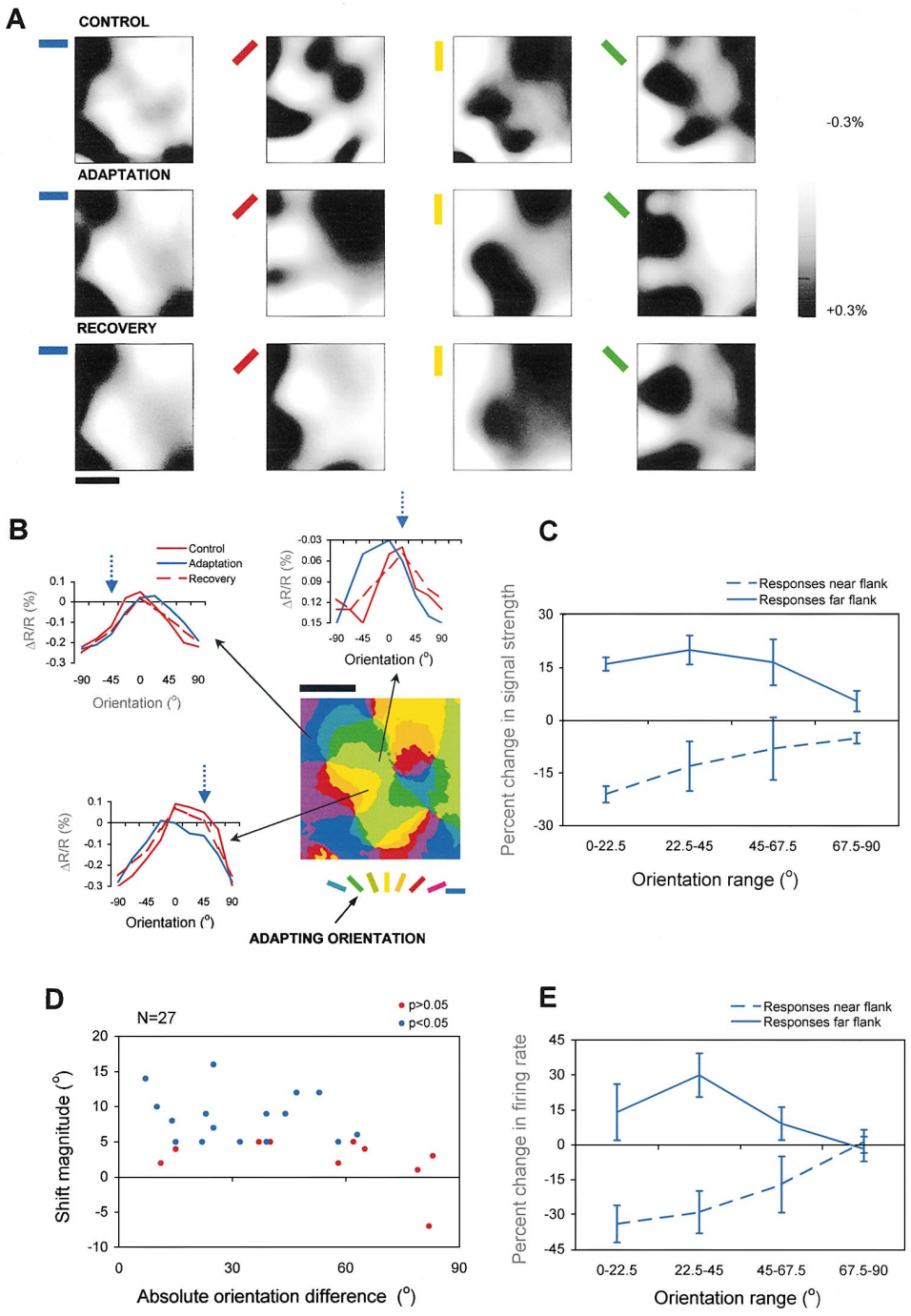

Figure 5. Changes in Signal Strength Induced by Adaptation

(A) Single-orientation responses during control, adaptation, and recovery. Colored bars on the top left of each map indicate four orientations: 0°, 45°, 90°, and 135° from a total of eight presented during control and adaptation and four during recovery. The gray scale on the right represents changes in light reflectance ΔR/R (signal strength), where R is the blank response for each condition (see Experimental Procedures). For display purposes, all single-condition maps were smoothed using a low-pass filter (the range of ΔR/R values did not differ between the control, adaptation, and recovery conditions). Signal analysis was performed only using unfiltered maps. Scale bar is 0.5 mm.

(B) Representative tuning curves of pixels showing adaptation-induced response suppression on the near flank and response facilitation on the far flank. Orientation tuning curves were calculated during the control condition (red), after 1 hr of continuous adaptation (blue), and during recovery (red, dashed line). They were derived from eight single-orientation maps (orientation resolution, 22.5°) during control and adaptation, and from four single-orientation maps (orientation resolution, 45°) during recovery (we have interpolated the four-orientation tuning curves during recovery using linear interpolation to obtain tuning curves with eight orientations spaced at 22.5°). The adapting orientation is marked by the blue arrow (135°). The location of each pixel is marked by a black arrow. In the tuning curve display convention, the control optimal orientation is represented as 0°, and the tuning curves after adaptation are represented relative to the control condition. The composite map

actively and nonlinearly by the temporal context of stimulation. Previous examination of the effect of temporal context pertains to studies that have demonstrated that adapting neurons to a potent stimulus can reduce responses to subsequent similar stimuli. This property has been characterized with respect to many stimulus dimensions, such as orientation (Blakemore and Campbell, 1969; Hammond et al., 1989; Nelson, 1991; Carandini et al., 1998; Muller et al., 1999), contrast (Movshon and Lennie, 1979; Ohzawa et al., 1982; Carandini and Ferster, 1997; Carandini et al., 1997), spatial frequency (Movshon and Lennie, 1979; Saul and Cynader, 1989), direction of motion (Maffei et al., 1973; Hammond et al., 1985, 1986), and velocity (Hammond et al., 1985). Saul and Cynader (1989) have demonstrated that pattern adaptation causes changes in the spatial frequency tuning of a small group of V1 neurons, an effect that is related to the changes in orientation preference reported here. However, it is generally assumed that in the orientation domain adaptation reduces responses at all orientations, the maximum reduction being obtained when the cell's preferred orientation and that of the adapting stimulus are the same (this property can be generalized to most stimulus attributes). A reduction of responses may result from mechanisms at the level of individual neurons, such as tonic hyperpolarization of the membrane potential of V1 cells (Carandini and Ferster, 1997), due possibly to synaptic depression (Abbott et al., 1997; Chance et al., 1998) or to slow hyperpolarizing Ca^{2+}- and Na^{2+}-activated potassium channels (Sanchez-Vives et al., 2000). The changes in orientation selectivity reported here, i.e., shifts in orientation preference by depression of responses on the near flank and facilitation of responses on the far flank, imply a network mechanism that reorganizes responses across a broad range of orientations, possibly through changes in the gain of local cortical circuits that mediate recurrent excitation and inhibition (Ben-Yishai et al., 1995; Douglas et al., 1995; Somers et al., 1995) and include disinhibitory mechanisms (Dragoi and Sur, 2000). For example, if the local cortical circuit includes broadly tuned orientation inhibition, hyperpolarization of neurons representing the adapting orientation could cause disinhibition of responses on the far flank of the tuning curve in the recorded neuron, an effect that could be further amplified via local excitatory interactions.

Our data also provide insight into the neural substrate of changes in perceived orientation induced by temporal context. Although these perceptual orientation aftereffects, e.g., the tilt aftereffect (Gibson, 1933; Gibson and Radner, 1937; Magnussen and Kurtenbach, 1980; Wolfe, 1984; Greenlee and Magnussen, 1987), have been known for a long time and several explanations have been offered (such as lateral inhibition between orientation detectors in visual cortex [Ganz, 1966; Tolhurst and Thompson, 1975] or "fatigue" of cortical neurons [Kohler and Wallach, 1944; Blakemore and Campbell, 1969; Blakemore and Nachmias, 1971]), the underlying neural mechanisms have been unclear. In the light of our results, we propose that such orientation aftereffects may be explained by plasticity in the preferred orientation of visual cortical cells induced by the temporal context of stimulation. The increase in cortical responses around the new preferred orientation predicts that long-term adaptation (over a time course of minutes) can improve the detectability of oriented contours tilted away from the adapting stimulus. Short-term adaptation, which leads to a reduction in the mean response, has been proposed to improve orientation discrimination by reducing correlations among responses of cell populations (Barlow, 1990; Müller et al., 1999). Our demonstration that long-term adaptation causes a reorganization of orientation-selective responses, including a supraoptimal increase in responses around the new preferred orientation, suggests an additional mechanism (Wainwright, 1999) for improving information transmission such that visual cortical neurons maintain a high level of discriminability in the face of prolonged exposure to the statistics of natural images (Coppola et al., 1998; Whitaker and McGraw, 2000).

Experimental Procedures

Animals

Nine adult cats were used in these experiments. All experiments were performed under protocols approved by MIT's Animal Care and Use Committee. Anesthesia was induced with ketamine (15 mg/kg, intramuscular [im]) and xylazine (1.5 mg/kg, im) and maintained with isofluorane (typically 0.5%–1.5% in 70/30 mixture of N_2O/O_2) delivered through a tracheal cannula. Cats were paralyzed with intravenous norcuron (2.2 mg/kg) and artificially respired to maintain end-tidal CO_2 at $\sim$4% at a partial pressure of 30 $\pm$ 3 mm Hg. The animals' EEG and EKG were monitored continuously to ensure adequate anesthesia. Craniotomy followed by durotomy was performed to expose primary visual cortex. Contact lenses were used to focus the eyes on a computer monitor.

Electrophysiology

We measured the neuronal response to 16 drifting high-contrast square-wave gratings. Stimuli were presented at orientations 22.5°

in (B) exhibited postadaptation repulsive shifts in the orientation preference of pixels, similar to those described in Figure 4, and then fully recovered from adaptation.

(C) Percent change in signal strength for each orientation domain from the map represented in Figure 5B. After orientation tuning curves were calculated for each orientation domain during the control condition and after 1 hr of adaptation (using mean $\Delta R/R$ values), we evaluated the adaptation-induced changes in signal strength on the near (dashed line) and far (solid line) flanks relative to the adapting orientation. The x axis represents absolute orientation difference range between each domain's preferred orientation and that of the adapting stimulus ($\Delta\theta$). As for the single-unit data (Figures 2D and 2E), we averaged changes in domains with symmetric $\Delta\theta$s. Both suppressive effects on the near flank and facilitatory effects on the far flank recovered from adaptation.

(D) Scatter plot ($n = 27$ cells) showing the magnitude of the shift in preferred orientation after 1 hr of continuous adaptation, for a duration identical to imaging experiments, as a function of the absolute difference between the control-preferred orientation and that of the adapting stimulus. Cells that show significant shifts in preferred orientation are shown in blue ($p < 0.05$); those that do not show significant shifts are shown in red ($p > 0.05$).

(E) Percent change in firing rate of responses on the near and far flanks of the tuning curve relative to the adapting orientation. The x axis is identical to that in Figure 5B. Each graph represents mean values $\pm$ SEM.

apart, each at two opposite directions of movement. Typical stimulus parameters for V1 were: spatial frequency, 0.5 cycle/degree; temporal frequency, 1 Hz. All stimuli were randomly interleaved. Stimuli were presented binocularly and were shown to the animal on a 17 inch monitor positioned 30 cm in front of it. We recorded responses during 5 conditions: (1) before adaptation (control), when 16 drifting gratings were presented for 10 trials each for a total of 160 trials, 2.5 s each presentation; (2) during 2 min of continuous adaptation to one grating of fixed orientation moving randomly in two opposite directions—the drifting adapting stimulus, which was presented at a temporal frequency of 1 Hz, changed its direction of motion randomly every 30 s (each direction was presented continuously for at least 30 s of adaptation); (3) after adaptation, when each of the 16 gratings presented for 112 trials, 2.5 s each presentation, was preceded by a 5 s "topping-up" presentation of the adapting orientation in order to maintain the effects of previous adaptation (Movshon and Lennie, 1979; Carandini et al., 1998); (4) during 10 min of recovery, when a full-field uniform stimulus was presented; and (5) after recovery, when 16 gratings were presented in identical conditions as in the control condition. The full protocol, including control, adaptation, and recovery periods, lasted about 2 hr. Single-unit extracellular recordings were made using tungsten microelectrodes (1.5–2 MΩ resistance) that were advanced through the cortex using a pulse motor microdrive (Narishige Scientific Instruments Lab). The signal was amplified using an 8-channel differential amplifier (DataWave Technologies), thresholded using an amplitude discriminator, displayed on an oscilloscope (Tektronix TDS 210), and played over an audio monitor (Optimus). We recorded at cortical depths between 500 and 1500 μm from cells with initial orientation preferences covering the entire orientation range (between 0° and 180°).

The preferred orientation was calculated as described previously (Wörgötter and Eysel, 1991). The Fourier components were extracted from the orientation tuning curve and then normalized by dividing by the mean firing rate of the cell during stimulus presentation:

$$a = \Sigma_{i=0}^{N-1} R(\theta_i)\cos(2\theta_i);\ b = \Sigma_{i=0}^{N-1} R(\theta_i)\sin(2\theta_i),$$

where responses, $R(\theta_i)$, are obtained for a set of N test orientations θ_i, $i = 0, 1 \ldots N-1$, which are uniformly distributed over 0°–180°, after averaging responses to the opposite directions of movement. Preferred orientation, θ, is calculated as

$$\theta = 0.5\arctan(b/a) \text{ if } a > 0 \text{ or } \theta = 180 + 0.5\arctan(b/a) \text{ if } a < 0.$$

This method, also known as vector averaging, allows one to estimate the preferred orientation if the measured responses are equally spaced in the orientation domain across a full 180° or 360° range without requiring an actual fit of the tuning curve (see Swindale, 1998, for a review of empirical descriptions and parameter estimation for orientation tuning curves). For each cell we calculated the percent change in firing rate by comparing responses at the preadaptation preferred orientation during control and adaptation conditions, after subtraction of the DC component. The orientation selectivity index (OSI), which measures the strength of orientation tuning, is given by $OSI = c/(\text{Mean Firing})$, where $c = \sqrt{(a^2 + b^2)}$ and Mean Firing is the mean response magnitude averaged over all orientations (Wörgötter and Eysel, 1991).

The adaptation time course protocol involved recording cortical responses in the following conditions: (1) control, 160 trials, identical to the control condition described previously; (2) successive sessions of continuous adaptation to one grating of fixed orientation that was randomly drifting in both directions (presented for 10 s, 2 min, and 10 min), followed by 112 trials in which all gratings were randomly interleaved (each one of the 16 gratings was preceded by a 5 stopping-up presentation of the adapting orientation); (3) successive recovery sessions, identical to that described above, lasting for 10 s, 10 min, and 20 min, followed by 112 trials in which all gratings were presented in conditions identical to the control. The entire duration of the protocol was about 3.5 hr. The extracellular recordings paralleling the optical imaging experiments were performed using the same adaptation protocol, except for the adaptation time, which was set to 1 hr.

Optical Imaging

Techniques for intrinsic signal imaging were similar to those described previously (Sheth et al., 1996; Rao et al., 1997; Toth et al., 1997). A stainless steel recording chamber (18 mm diameter, calculated at coordinate P5.0) was attached to the skull surrounding the craniotomy, filled with silicone oil, and then sealed with a quartz plate. A video camera (CCD-5024N Bishke, Japan, RS-170, >60 dB signal-to-noise ratio) consisting of a 655 by 480 array of pixels equipped with a tandem-lens macroscope was positioned over the cortex. This arrangement gave a magnification of 75 pixels/mm. Data were collected using an imaging system (Optical Imaging). The camera signal was amplified by a video enhancement amplifier; a baseline image was subtracted from each stimulus response image in analog form and then digitized. Light from a 100 W tungsten halogen light source driven by a DC power supply (Kepco) was passed through a filter and used to illuminate the cortex. Initially, a reference map of blood vessel pattern at the surface of the cortex was obtained by using light at 550 ± 40 nm. The camera was then focused 400–500 μm below the surface of the cortex and data collected using light at 610 nm. Frames were summed between 0.5 and 3.5 s after stimulus onset, corresponding to the time of maximum signal as determined previously (Rao et al., 1997; Sheth et al., 1996). Data were analyzed using in-house programs written in Matlab.

Stimuli for optical imaging experiments were identical to those used in the extracellular recording. However, because of the much slower time course of the intrinsic signals, we could not replicate the same adaptation protocol as during single-unit recording, presenting instead the adapting stimulus continuously for about 1 hr. This value was chosen after conducting preliminary experiments to determine the minimum adaptation time that induces plasticity that would persist during the imaging after adaptation (adaptation and recovery conditions), which lasts ~3 hr. After adaptation, intrinsic signals were imaged by presenting the same stimuli as in the control condition. Next, after 1 hr of presenting a full-field uniform stimulus, we tested the effect of recovery. Orientation maps during control, adaptation, and recovery were obtained by averaging the optical signal acquired during 72 trials in each condition (single-orientation responses) and then dividing them by responses to the blank screen (Grinvald et al., 1986; Sheth et al., 1996; Rao et al., 1997; Toth et al., 1997) (data treatment was identical during control, adaptation, and recovery). Before conducting the adaptation experiments, we determined the reproducibility of optical imaging orientation maps within the same animal. Our analyses yielded reliable maps of orientation preference, with a mean pixel orientation change of 3.8° for maps obtained 7 hr apart.

Acknowledgments

We thank Casto Rivadulla, James Schummers, and Al Lyckman for critical discussions of previous versions of this manuscript. Supported by NIH grant EY07023.

Received May 17, 2000; revised August 22, 2000.

References

Abbott, L.F., Varela, J.A., Sen, K., and Nelson, S.B. (1997). Synaptic depression and cortical gain control. Science *275*, 220–224.

Barlow, H.B. (1990). A theory about the functional role and synaptic mechanism of after-effects. In Vision: Coding and Efficiency, C. Blakemore, ed. (Cambridge: Cambridge Univ. Press), pp. 363–375.

Benevento, L.A., Creutzfeldt, O.D., and Kuhnt, U. (1972). Significance of intracortical inhibition in the visual cortex. Nat. New Biol. *238*, 124–126.

Ben-Yishai, R., Bar-Or, R.L., and Sompolinsky, H. (1995). Theory of orientation tuning in visual cortex. Proc. Natl. Acad. Sci. USA *92*, 3844–3848.

Blakemore, C. (1977). Genetic instructions and developmental plasticity in the kitten's visual cortex. Phil. Trans. R. Soc. Lond. B Biol. Sci. *278*, 425–434.

Blakemore, C., and Campbell, F.W.J. (1969). Adaptation to spatial stimuli. J. Physiol. Lond. *200*, 11P–13P.

Blakemore, C., and Cooper, G.F.D. (1970). Development of the brain depends on the visual environment. Nature *228*, 477–478.

Blakemore, C., and Nachmias, J. (1971). The orientation specificity of two visual after-effects. J. Physiol. Lond. *213*, 157–174.

Carandini, M., and Ferster, D. (1997). A tonic hyperpolarization underlying contrast adaptation in cat visual cortex. Science *276*, 949–952.

Carandini, M., Barlow, H.B., O'Keefe, O.P., Poirson, A.B., and Movshon, J.A. (1997). Adaptation to contingencies in macaque primary visual cortex. Phil. Trans. R. Soc. Lond. B Biol. Sci. *352*, 1149–1154.

Carandini, M., Movshon, J.A., and Ferster, D. (1998). Pattern adaptation and cross-orientation interactions in the primary visual cortex. Neuropharmacology *37*, 501–511.

Celebrini, S., Thorpe, S., Trotter, Y., and Imbert, M. (1993). Dynamics of orientation coding in area V1 of the awake primate. Vis. Neurosci. *10*, 811–825.

Chance, F.S., Nelson, S.B., and Abbott, L.F. (1998). Synaptic depression and the temporal response characteristics of V1 cells. J. Neurosci. *18*, 4785–4799.

Crair, M.C., Gillespie, D.C., and Stryker, M.P. (1998). The role of visual experience in the development of columns in cat visual cortex. Science *279*, 566–570.

Chapman, B., Zahs, K.R., and Stryker, M.P. (1991). Relation of cortical cell orientation selectivity to alignment of receptive fields of the geniculocortical afferents that arborize within a single orientation column in ferret visual cortex. J. Neurosci. *11*, 1347–1358.

Coppola, D.M., Purves, H.R., McCoy, A.N., and Purves, D. (1998). The distribution of oriented contours in the real world. Proc. Natl. Acad. Sci. USA *95*, 4002–4006.

Douglas, R.J., Koch, C., Mahowald, M., Martin, K.A.C., and Suarez, H.H. (1995). Recurrent excitation in neocortical circuits. Science *269*, 981–985.

Dragoi, V., and Sur, M. (2000). Dynamic properties of recurrent inhibition in primary visual cortex: contrast and orientation dependence of contextual effects. J. Neurophysiol. *83*, 1019–1030.

Ferster, D. (1986). Orientation selectivity of synaptic potentials in neurons of cat primary visual cortex. J. Neurosci. *6*, 1284–1301.

Ferster, D., Chung, S., and Wheat, H. (1996). Orientation selectivity of thalamic input to simple cells of cat visual cortex. Nature *21*, 249–252.

Fregnac, Y., and Imbert, M. (1978). Early development of visual cortical cells in normal and dark-reared kittens: relationship between orientation selectivity and ocular dominance. J. Physiol. Lond. *278*, 27–44.

Ganz, L. (1966). Mechanisms of figural after-effects. Psychol. Rev. *73*, 128–150.

Gibson, J.J. (1933). Adaptation, after-effect and contrast in the perception of curved lines. J. Exp. Psychol. *16*, 1–33.

Gibson, J.J., and Radner, M. (1937). Adaptation, after-effect and contrast in the perception of tilted lines. I Quantitative studies. J. Exp. Psychol. *20*, 453–467.

Godecke, I., Kim, D.S., Bonhoeffer, T., and Singer, W. (1997). Development of orientation preference maps in area 18 of kitten visual cortex. Eur. J. Neurosci. *9*, 1754–1762.

Greenlee, M.W., and Magnussen, S. (1987). Saturation of the tilt aftereffect. Vision Res. *27*, 1041–1043.

Grinvald, A., Lieke, E., Frostig, R.D., Gilbert, C.D., and Wiesel, T.N. (1986). Functional architecture of cortex revealed by optical imaging of intrinsic signals. Nature *324*, 361–364.

Hammond, P., Mouat, G.S., and Smith, A.T. (1985). Motion after-effects in cat striate cortex elicited by moving gratings. Exp. Brain Res. *60*, 411–416.

Hammond, P., Mouat, G.S., and Smith, A.T. (1986). Motion after-effects in cat striate cortex elicited by moving texture. Vision Res. *26*, 1055–1060.

Hammond, P., Pomfrett, C.J., and Ahmed, B. (1989). Neural motion after-effects in the cat's striate cortex: orientation selectivity. Vision Res. *29*, 1671–1683.

Hirsch, H.V., and Spinelli, D.N. (1970). Visual experience modifies distribution of horizontally and vertically oriented receptive fields in cats. Science *168*, 869–871.

Hubel, D.H., and Wiesel, T.N. (1962). Receptive fields, binocular interaction and functional architecture in the cat's visual cortex. J. Physiol. Lond. *160*, 106–154.

Hubel, D.H., and Wiesel, T.N. (1963). Receptive fields of cells in striate cortex of very young, visually inexperienced kittens. J. Neurophysiol. *26*, 994–1002.

Kohler, W., and Wallach, H. (1944). Figural after-effects: an investigation of visual responses. Proc. Amer. Phil. Soc. *88*, 306–335.

Maffei, L., Fiorentini, A., and Bisti, S. (1973). Neural correlate of perceptual adaptation to gratings. Science *182*, 1036–1038.

Magnussen, S., and Kurtenbach, W. (1980). Adapting to two orientations: disinhibition in a visual after effect. Science *207*, 908–909.

Movshon, A., and Lennie, P. (1979). Pattern-selective adaptation in visual cortical neurones. Nature *278*, 850–852.

Müller, J.R., Metha, A.B., Krauskopf, J., and Lennie, P. (1999). Rapid adaptation in visual cortex to the structure of images. Science *285*, 1405–1408.

Nelson, S.B. (1991). Temporal interactions in the cat visual system. I. Orientation-selective suppression in the visual cortex. J. Neurosci. *11*, 344–356.

Ohzawa, I., Sclar, G., and Freeman, R.D.S. (1982). Contrast gain control in the cat visual cortex. Nature *298*, 266–268.

Rao, S.C., Toth, L.J., and Sur, M. (1997). Optically imaged maps of orientation preference in primary visual cortex of cats and ferrets. J. Comp. Neurol. *387*, 358–370.

Reid, R.C., and Alonso, J.M. (1995). Specificity of monosynaptic connections from thalamus to visual cortex. Nature *378*, 281–284.

Ringach, D.L., Hawken, M.J., and Shapley, R. (1997). Dynamics of orientation tuning in macaque primary visual cortex. Nature *387*, 281–284.

Sanchez-Vives, M.V., Nowak, L.G., and McCormick, D.A. (2000). Membrane mechanisms underlying contrast adaptation in cat area 17 in vivo. J. Neurosci. *20*, 4267–4285.

Saul, A.B., and Cynader, M.S. (1989). Adaptation in single units in visual cortex: the tuning of aftereffects in the spatial domain. Vis. Neurosci. *2*, 593–607.

Sengpiel, F., Stawinski, P., and Bonhoeffer, T. (1999). Influence of experience on orientation maps in cat visual cortex. Nat. Neurosci. *2*, 727–732.

Sheth, B.R., Sharma, J., Rao, S.C., and Sur, M. (1996). Orientation maps of subjective contours in visual cortex. Science *274*, 2110–2115.

Shevelev, I.A., Sharaev, G.A., Lazareva, N.A., Novikova, R.V., and Tikhomirov, A.S. (1993). Dynamics of orientation tuning in the cat striate cortex neurons. Neuroscience *56*, 865–876.

Sillito, A.M., Kemp, J.A., Milson, J.A., and Berardi, N. (1980). A re-evaluation of the mechanisms underlying simple cell orientation selectivity. Brain Res. *194*, 517–520.

Somers, D.C., Nelson, S.B., and Sur, M. (1995). An emergent model of orientation selectivity in cat visual cortical simple cells. J. Neurosci. *15*, 5448–5465.

Stryker, M.P., Sherk, H., Leventhal, A.G., and Hirsch, H.V. (1978). Physiological consequences for the cat's visual cortex of effectively restricting early visual experience with oriented contours. J. Neurophysiol. *41*, 896–909.

Swindale, N.V. (1998). Orientation tuning curves: empirical description and estimation of parameters. Biol. Cybern. *78*, 45–56.

Tolhurst, D.J., and Thompson, P.G. (1975). Orientation illusions and after-effects: inhibition between channels. Vision Res. *15*, 967–972.

Toth, L.J., Kim, D.S., Rao, S.C., and Sur, M. (1997). Integration of local inputs in visual cortex. Cereb. Cortex *7*, 703–710.

Wainwright, M.J. (1999). Visual adaptation as optimal information transmission. Vision Res. *39*, 3960–3974.

Whitaker, D., and McGraw, P.V. (2000). Long-term visual experience recalibrates human orientation perception. Nat. Neurosci *3*, 13.

Wolfe, J.M. (1984). Short test flashes produce large tilt aftereffects. Vision Res. *24*, 1959–1964.

Wörgötter, F., and Eysel, U.T. (1991). Correlations between directional and orientational tuning of cells in cat striate cortex. Exp. Brain Res. *83*, 665–669.

Wörgötter, F., and Koch, C. (1991). A detailed model of the primary visual pathway in the cat: comparison of afferent excitatory and intracortical inhibitory connection schemes for orientation selectivity. J. Neurosci. *11*, 1959–1979.